Characteristics of Guided and Leaky Waves on Multilayer Thin-Film Structures with Planar Material Gratings

Hung Yu David Yang, *Senior Member, IEEE*

***Abstract*— This paper presents the characteristics of guided (surface) waves and leaky waves on multilayer structures with planar implanted periodic dielectric blocks. A three-dimensional (3–D) integral-equation formulation in conjunction with the method of moments (MoM's) is used to find the propagation constants of the surface-wave and leaky-wave modes. The analysis deals with layered structures with irregular implants. Photonic band-gaps of both guided waves and leaky waves for rectangular air-implants are identified. Anisotropic properties of the surface waves and leaky waves are investigated. The design of leaky-wave antennas with the information of mode characteristics is discussed. The analysis is validated through the comparison with a low-frequency effective-medium approach and results for linear gratings.**

***Index Terms*—Dielectric films, gratings, leaky waves, photonics, surface waves.**

I. Introduction

DUE TO THE RECENT advances of material technology, there are growing research activities on the electromagnetic applications of advanced (artificial) materials. Many technologies will benefit if the electric or optical properties of materials can be properly controlled. Photonic crystals where wave propagation is prohibited within a certain band are examples of such applications [1]. In addition, thin-film structures containing periodic material implants (gratings) have been of considerable interest in integrated optics [2], leaky-wave antennas [3], frequency-selective surfaces [4], [5], and absorbing materials [6], [7]. In the past, there has been considerable work on material-layered structures with material gratings, mostly for two-dimensional (2-D) structures with gratings in one direction. References [8]–[11] are some of the examples. Layer structures with 2-D gratings had also been investigated, but mostly for scattering applications, such as for frequency-selective surfaces [4], [5] and absorbers [6], [7]. In recent years, due to the advances of micromachining technology, layered thin-film structures with planar material gratings are becoming applicable and have many potential millimeter-wave and optical applications, such as planar-distributed Bragg reflection devices and planar leaky-wave antennas. The implementation of photonic band-gap materials in integrated circuit and antenna structures may open up many possibilities of useful devices. The properties of surface and leaky waves on a layered structure with planar material gratings provide the explanation of many fundamental physical phenomena of the associated devices.

In this paper, a three-dimensional (3–D) integral-equation formulation in conjunction with the method of moments (MoM's) is applied to the electromagnetic boundary value problems of dielectric-layered structures with planar periodic material implants. The integral equation and the associated dyadic Green's function for layered periodic structures are described in Section II and the Appendix. The MoM and numerical consideration are described in Section III. Results for surface-wave (bounded) and leaky-wave characteristics as a function of material and geometric parameters including the planar-direction angle are discussed in Section IV. Photonic band structures for selected examples of planar grating structures are also illustrated.

II. Periodic Dyadic Green's Function Formulation

Although the analysis can be easily extended to more layers with multiple implants, the formulation in this work is limited to a three-layer structure with planar material gratings within the middle layer shown in Fig. 1. The geometry is assumed to consist of infinite planar arrays of material blocks within a surrounding layer. The top region is air and the bottom region can be either a substrate or a conductor ground. Although the implants shown in Fig. 1 are rectangular blocks, the developed analysis is general enough for most irregular implants. If the implanted material has a dielectric constant ε_e, Maxwell's curl equations for time-harmonic fields within the supporting layer (dielectric constant ε_2) can be written as

$$\nabla \times \vec{E} = -j\omega\mu_0\vec{H} \tag{1}$$

and

$$\nabla \times \vec{H} = -j\omega\varepsilon_0(\varepsilon_e - \varepsilon_2)\zeta(\vec{r})\vec{E} + j\omega\varepsilon_2\varepsilon_0\vec{E}. \tag{2}$$

$\zeta(\vec{r})$ is a unity function within the material implants and zero elsewhere. The first term at the right-hand side (RHS) of (2) is treated as the displacement current and is noted as $\vec{J}_e$ that exists only within the implants. The electric-field integral equation for the pertinent problem is

$$\vec{E} = \iiint_v [G] \cdot \vec{J}_e \, dv' \tag{3}$$

Manuscript received July 22, 1996; revised November 21, 1996. This work was supported in part by a contract from Phraxos Research and Development, Inc.

The author is with the Department of Electrical Engineering and Computer Science, University of Illinois at Chicago 60607-7053 USA.

Publisher Item Identifier S 0018-9480(97)01711-0.

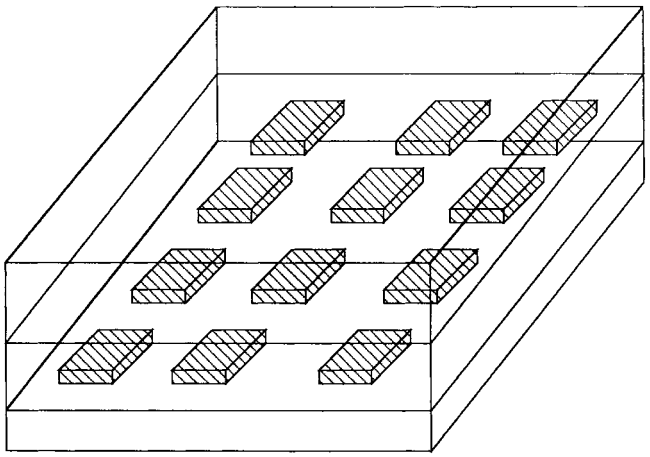

Fig. 1. Geometry of infinite planar arrays of dielectric blocks in a multilayer structure.

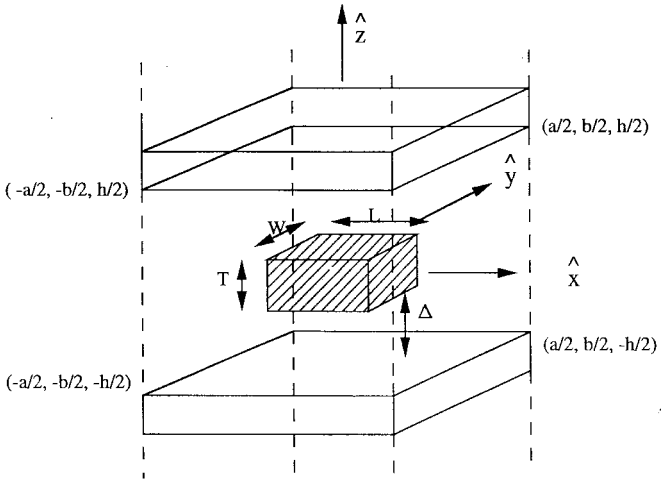

Fig. 2. A unit cell of 2-D periodic material blocks within layered media.

which is established to express electric fields in terms of displacement currents. The volume integral is over only the region of implanted material blocks centered at the origin of the Cartesian coordinates. The electric fields within the material block at a unit cell are the unknowns in the MoM analysis. Since all three components of the fields are involved, it is necessary to deal with a full dyadic Green's function for layered media expressed as

$$[G] = \begin{bmatrix} G_{xx} & G_{xy} & G_{xz} \\ G_{yx} & G_{yy} & G_{yz} \\ G_{zx} & G_{zy} & G_{zz} \end{bmatrix}. \tag{4}$$

Since the structure is periodic, Floquet's theorem is applied to simplify the problem to the modeling of electromagnetic waves within an infinitely long cylinder shown in Fig. 2. The boundary conditions at the surface of the unit cell are determined by the Floquet's theorem. The cross section of the rectangular cylinder extends within $-a/2 \le x \le a/2$ and $-b/2 \le y \le b/2$. A material block is at the center of the cell with length L (along the $\hat{x}$ axis), width W (along the $\hat{y}$ axis), and the thickness T (along the $\hat{z}$ axis). The supporting layer with thickness h extends from $-h/2$ to $h/2$. Δ is the distance measured from the bottom of the block to the layer interface (see Fig. 2). For planar periodic structures, the components of the dyadic Green's function in terms of Floquet modes (plane-wave expansion) [12] may be expressed as

$$G_{uv} = \frac{1}{ab} \sum_{m=-\infty}^{\infty} \sum_{n=-\infty}^{\infty} \tilde{G}_{uv}\, e^{-jk_x(x-x')-jk_y(y-y')} \tag{5}$$

where $k_x = 2m\pi/a + \beta_x$ and $k_y = 2n\pi/b + \beta_y$. u or v is either x, y, or z. β_x and β_y are the propagation constants in the x and y directions, respectively. $\tilde{G}_{uv}$ is the spectral Green's function component and is a function of spectral variables k_x and k_y, z,z', and the material parameters. This spectral Green's function for a multilayer structure is derived with a spectral matrix method [13] and is described in the Appendix.

III. The MoM and Numerical Consideration

A finite-element MoM procedure is applied numerically to determine the electric fields within the material implants. This is done first by discretizing the material implants into many small cells within which the fields are assumed constants, but with unknown coefficients

$$\vec{E} = \sum_{m_x=1}^{M_x} \sum_{m_y=1}^{M_y} \sum_{m_z=1}^{M_z} \vec{A}_{m_x m_y m_z} f(m_x, m_y, m_z) \tag{6}$$

where within the cell (m_x, m_y, m_z), $f(m_x, m_y, m_z) = 1$ and $f = 0$, elsewhere. There are M_x, M_y, and M_z divisions in each side of the material blocks (the x, y, and z directions, respectively). If the field representation in (6) is used in the vector integral equation and the resulting fields are evaluated at the cell at indices m_x, m_y, and m_z, respectively, for the x, y, and z directions, the integral equations are converted into a set of linear equations (a matrix equation):

$$\vec{A}_i = \sum_j \sum_{m=-\infty}^{\infty} \sum_{n=-\infty}^{\infty} [g]_{\text{ijmn}} \cdot \vec{A}_j (\varepsilon_e - \varepsilon_2) \tag{7}$$

where each i or j represents a particular field component at a cell and $[g]_{\text{ijmn}}$ is a 3×3 matrix resulting from two volume integrals over the cells associated with i and j in the MoM procedure. The center of the rectangular cell for an expansion mode is $\vec{r}_j$ and for a testing mode is $\vec{r}_i$ with $\vec{r}_i = x_i\hat{x} + y_i\hat{y} + z_i\hat{z}$ and $\vec{r}_j = x_j\hat{x} + y_j\hat{y} + z_j\hat{z}$, and the cell size is Δx, Δy, and Δz in each of the three directions. $[g]_{\text{ijmn}}$ can be expressed as

$$[g]_{\text{ijmn}} = \frac{j\omega\varepsilon_0}{ab\Delta z^2} e^{-jk_x(x_i-x_j)} e^{-jk_y(y_i-y_j)} \cdot \frac{\sin^2\left(\frac{k_x\Delta x}{2}\right)}{\left(\frac{k_x\Delta x}{2}\right)^2} \frac{\sin^2\left(\frac{k_y\Delta y}{2}\right)}{\left(\frac{k_y\Delta y}{2}\right)^2} [Q]_{\text{ijmn}} \tag{8}$$

and

$$[Q]_{\text{ijmn}} = \int_{z_j-\Delta z/2}^{z_j+\Delta z/2} \int_{z_i-\Delta z/2}^{z_i+\Delta z/2} [\tilde{G}(k_x, k_y, z, z')]\, dz\, dz'. \tag{9}$$

The integration in (9) can be done analytically according to the procedures described in the Appendix. Analytic effort is

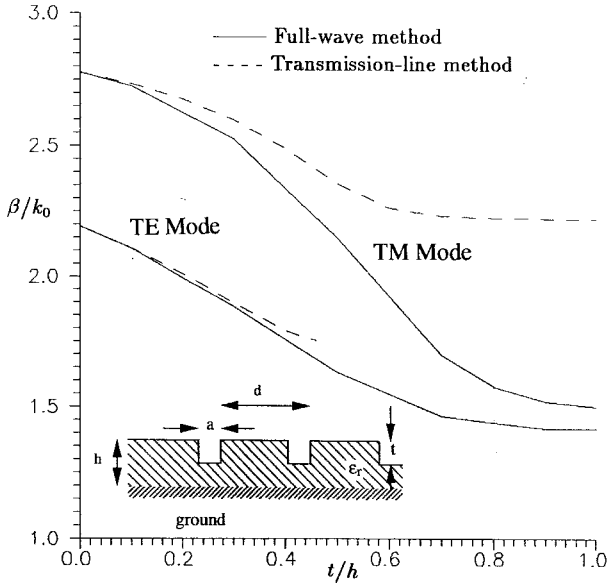

Fig. 3. Comparison of full-wave and transmission-line methods for guided-wave modes of a 1-D grating structure. $F = 15$ GHz, $\epsilon_r = 10, h = 3.18$ mm, $d = 3.25$ mm, $a = 1.58$ mm.

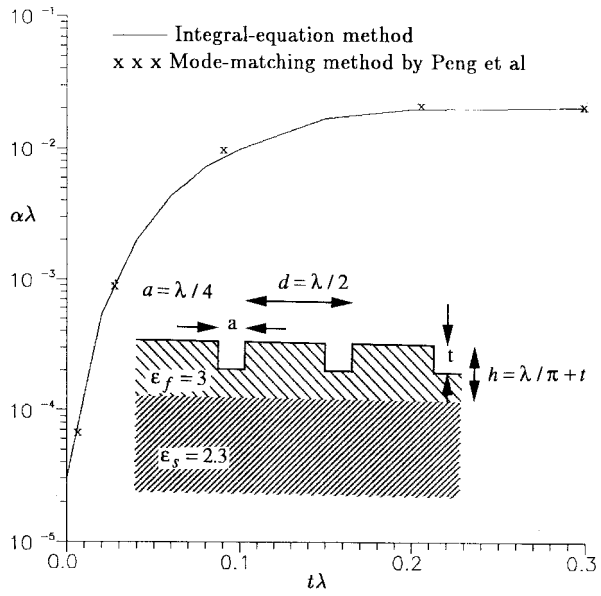

Fig. 4. Leaky-wave attenuation constant versus grating thickness for a 1-D grating structure.

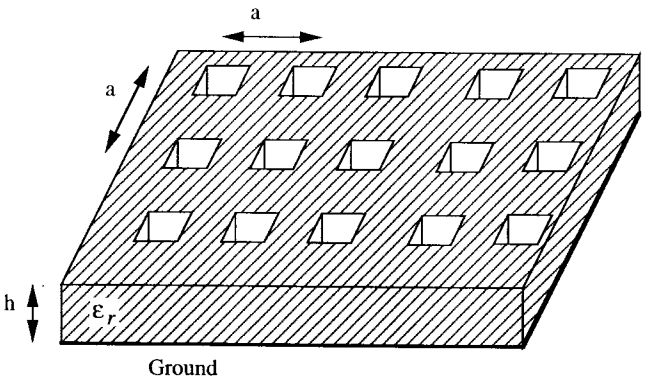

Fig. 5. The geometry of a grounded dielectric slab with planar periodic air blocks. The results in Table I and Figs. 6 and 7 are based on this structure. The parameters for Table I are $a = 3$ mm, $h = 3$ mm, $\varepsilon = 10, L = W = 1.0$ mm, and $T = 3.0$ mm.

required to ensure that there is no exponentially growing terms (as m or n becomes large) in the formulation. If both indices i and j run from 1 to $P = 3 \times M_x \times M_y \times M_z$, (7) represents a matrix equation with order P. A nontrivial solution for the fields requires the matrix determinant to be zero, which results in a characteristic equation. The eigenvalues (propagation constants) β are obtained from the roots of this equation. For a lossless structure, the propagation constant of a guided (surface) wave is a real number, and a bisection method for finding the roots of nonlinear functions is used. However, leaky-wave propagation constants are complex-valued and the Newton method is used for two real nonlinear equations with two unknowns (real and imaginary part of the complex propagation constant).

One of the features of the MoM is that the shape of the implants can be irregular. For instance, in the process of solving the matrix equations for rectangular blocks, one may set the displacement currents at some of the cells to zero. This procedure corresponds to physically cutting off pieces of the implants. An extensive validity check of the present analysis is performed. First, the implanted blocks are set as large as the unit cell so that the analytic results for the guided-wave modes and the plane-wave scattering are available. This test provides information regarding the number of expansion cells required for reasonable results.

The test is also performed for the cases of one-dimensional (1–D) gratings. In the analysis, if the implanted blocks are connected to one of the cell boundaries, the geometry reduces from 2-D to 1-D gratings. Compared here are the full-wave results of propagation constants of guide-waves against those with a transmission-line method [3]. The comparison is shown in Fig. 3. It is seen that the two methods agree well for shallow gratings. The discrepancies increase with the grating depth. In the transmission-line method, the grating structure is treated as the periodic cascades of two surface-waveguide sections, and all the higher order modes at the junctions are neglected. The junction (or higher order mode) effects become more important as the grating depth becomes larger. The validation is also performed for the attenuation constants of a leaky-wave mode in 1-D gratings. The results of the comparison between the integral-equation analysis in this paper and the mode-matching method described in [2] are shown in Fig. 4. The agreement is excellent.

The validation of the analysis is further checked against the effective-medium method, which is particularly accurate for low frequencies (cell size is much smaller than a wavelength). It has been shown in [14], [15] that a medium with infinitely long planar periodic rods can be approximated as a homogeneous medium with a uniaxial anisotropy. If dielectric constants of the supporting layer and the material blocks in Fig. 5 are ε_a and ε_b, respectively, and the thickness of the layer and blocks is the same, the dielectric constants of the

TABLE I
SURFACE-WAVE PHASE CONSTANT COMPARISON

Frequency (GHz)	β/k_0 (Full-Wave)	β/k_0 (Effective Medium)
2	1.007	1.007
4	1.035	1.035
6	1.124	1.123
7	1.237	1.232
8	1.430	1.422
9	1.678	1.665
10	1.061	1.050
	1.910	1.896

effective uniaxial material are

$$\varepsilon_z = (1-\chi)\varepsilon_a + \chi\varepsilon_b \tag{10a}$$

and

$$\varepsilon_t = \varepsilon_a + \frac{2\varepsilon_a(\varepsilon_b - \varepsilon_a)}{(1+\chi)\varepsilon_a + (1-\chi)\varepsilon_b}\chi. \tag{10b}$$

ε_t is the dielectric constant in the planar directions and χ is the area (normalized to the area of a unit cell) occupied by a material block and is defined as $(L \times W)/(a \times b)$. The test geometry is planar periodic air blocks carved on the surface of a grounded dielectric slab shown in Fig. 5. For the test case, the effective dielectric constants are $\varepsilon_z = 9.0$ and $\varepsilon_t = 8.33$, and the propagation constants are found from the characteristic equations for an anisotropic homogeneous grounded slab [16]. It is seen that the full-wave method agrees very well with the approximated effective-medium method, especially for lower frequencies.

It is observed that for higher the frequencies or larger the dimensions, more expansion cells are needed to obtained reasonable convergence. It is observed that the number of cells in the vertical (z) direction is more crucial. Generally, a vertical-cell size of about a tenth of the wave length provides reasonable convergence. In this paper, 1681 Floquet modes with $M_x = M_y = 3$ are used to produce the numerical results.

IV. RESULTS AND DISCUSSIONS

Guided waves and leaky waves on a dielectric-layered structure with 1-D material gratings have been well studied and their characteristics are understood. For 2-D material gratings, it is of interest to investigate the mode characteristics in various directions and the photonic band structures. An example of the dispersion diagram for guided- and leaky-wave modes of a grounded dielectric slab with 2-D rectangular material gratings (Fig. 5) is shown in Fig. 6 for propagation in the $\hat{x}$ direction (see Fig. 2). For the $\hat{x}$-direction waves, the mode characteristics are similar to the case of the 1-D grating. However, for planar grating structures, the modes are hybrid. There exist photonic band-gaps for modes near the Brillouin zone boundary. Since the structure is periodic, if β_x is a phase constant in the $\hat{x}$-direction, $\beta_x + 2n\pi/a$ for any integer n should also be the phase constant of the same wave. The Brillouin zone [17] is defined in k-space (phase-constant space) within which each wave has a unique phase constant. At low frequencies, the fundamental (hybrid) modes are similar

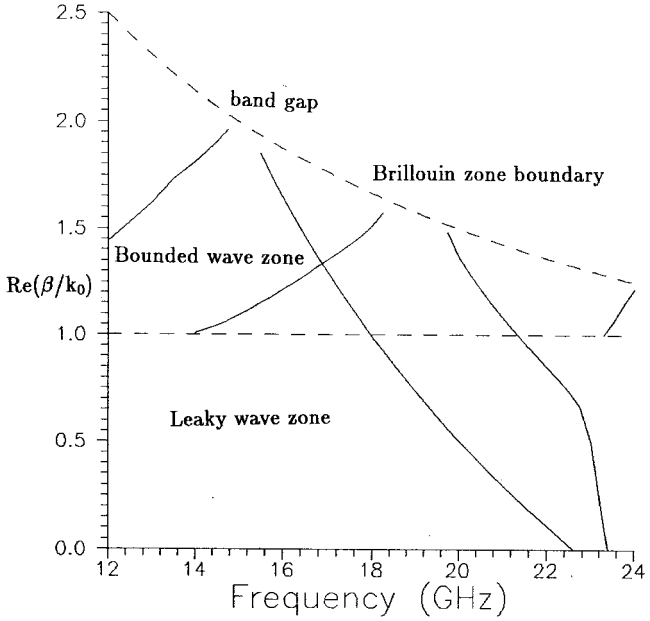

Fig. 6. Dispersion diagram for modes in a grounded slab with planar gratings (shown in Fig. 5). $h = 2$ mm, $T = 0.5$ mm, $\epsilon = 10$, $a = b = 5$ mm, $W = 3$ mm, and $L = 2.5$ mm. $\hat{x}$ is the propagation.

to a TM (upper) mode of a grounded dielectric slab. When the frequencies are such that the Bragg condition is satisfied, the bounded modes turn to complex-wave modes (band-gap zone). As frequency increases further, bounded surface-wave modes (in the slow-wave zone) turn into proper leaky wave modes (in the fast-wave zone). The frequency where the first leaky-wave mode turns on and the frequency band where only a single leaky-wave mode exist are of practical interest. These are determined by the profile of the gratings. It is known that the leaky-wave beam angle is determined mostly by the phase constant according to the formula [2]

$$\theta_m = \cos^{-1}\frac{\beta}{k_0}. \tag{11}$$

θ_m is measured from the horizon. It is seen from Fig. 6 that the fundamental leaky-wave phase constant decreases with frequency. Therefore, the beam angle increases with frequency as was demonstrated in Fig. 7. In Fig. 7, the beam angle versus frequency is shown for three different sets of grating width (W). The results are shown for the frequency range where only the fundamental leaky-wave mode exists. The results demonstrate the transverse-grating effects on leaky-wave characteristics. It is seen that the increase of the air-block width results in the increase of the leaky-wave turn-on frequency and the decrease of the beam angle (at a given frequency). The maximum beam angles without multiple beams are about the same for all the grating widths.

A contribution of this paper is the investigation of the characteristics of planar 2–D surface waves and leaky waves. These waves can be excited by microstrip elements on planar grating structures. An example of the phase constant of the fundamental surface-wave mode versus the directional angle is shown in Fig. 8. A given β_x and the corresponding β_y in Fig. 8 determine the propagation constant at a particular planar

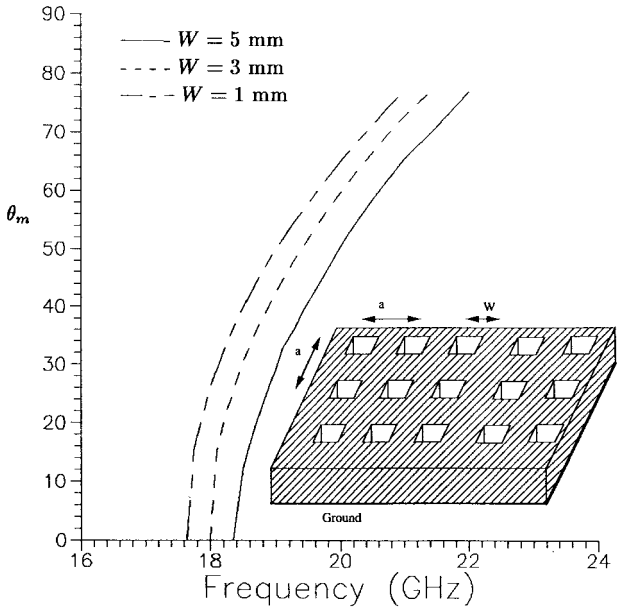

Fig. 7. Fundamental leaky-wave beam angle versus frequency. The leaky wave is propagating in the $\hat{x}$ direction. All other parameters are the same as those in Fig. 6 except the block width.

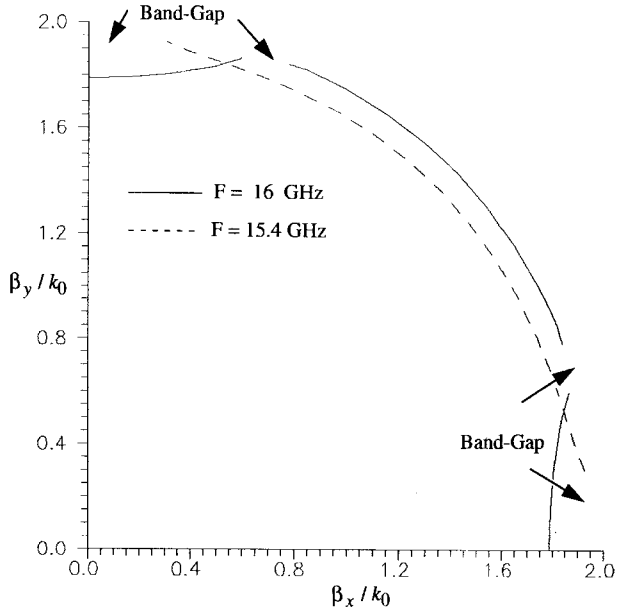

Fig. 8. Fundamental surface-wave phase constant for a grounded slab with planar gratings. $h = 2$ mm, $T = 1$ mm, $\varepsilon = 10, a = b = 5$ mm, and $L = W = 2.5$ mm.

direction (ϕ angle). Due to the symmetry, the irreducible Brillouin zone is for the ϕ angle from 0 to 45°. The results in Fig. 8 are for two different frequencies, 15.4 and 16 GHz. It is seen that there exist certain ranges of ϕ where propagating surface-wave modes vanish. Mathematically, the propagation constants are complex-valued in the propagation forbidden zone. It is seen that the wave forbidden zone varies with frequency. In contrast to the metal-clad dielectric slab with planar gratings where propagation may be prohibited in all directions [18], wave prohibition in *some* regions is found here—not *all* directions. The wave forbidden zone varies with frequencies. This implies that the structure can be used as a space-frequency signal selector.

Planar leaky-wave characteristics for a planar grating structure are investigated through the example shown in Fig. 9, where the leaky-wave phase constants are for a three-layer dielectric structure with planar air blocks embedded within the middle layer. It is seen that there exists an angle range (near $\phi = 45°$) where the leaky wave becomes a surface wave (the propagation constant is real and greater than k_0). This implies that there exists an angle range where the leaky wave is forbidden (null in leaky-wave antennas). The other interesting observation is that the leaky-wave phase constant varies significantly with direction (ϕ angle). This implies that as a leaky-wave antenna, the beam angle varies with each ϕ cut. It is possible, however, to arrange the shape of the unit cell of an infinite array of implants to minimize this beam-angle variation with ϕ.

It has been shown in [19] that there exists photonic band-gaps in 1-D material grating structures. It has also been shown in [18] that a complete photonic band-gap exists in planar material grating within a dielectric layer sandwiched by conductor plates. A question one would ask is "can an open planar material grating structure be constructed where guided

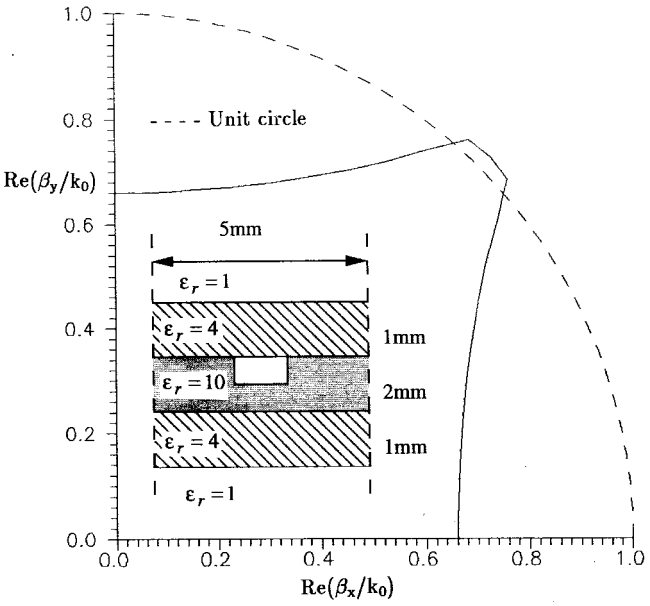

Fig. 9. Leaky-wave phase constant for a three-layer structure with planar periodic arrays of air blocks. $F = 20$ GHz, $T = 1$ mm, $a = b = 5$ mm, and $L = W = 3$ mm.

waves (surface waves) are prohibited in all directions?." This investigation cannot confirm that surface modes may be completely eliminated by using material gratings, but there is room for further research on this subject. A typical example of a surface-wave forbidden band versus direction angle is shown in Fig. 10. The example is for planar periodic material blocks on top of a conductor. It may be identified from Fig. 10, at a given frequency, the range of ϕ angles where guided waves are eliminated. The photonic band-gap at any given ϕ angle may also be found from Fig. 10.

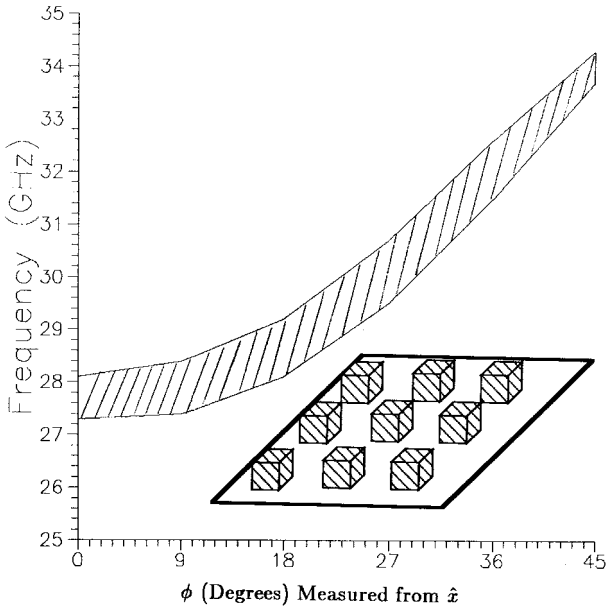

Fig. 10. Photonic band-gap versus wave propagation angle for planar periodic dielectric blocks on a ground plane. $T = 1$ mm, $a = b = 5$ mm, $L = W = 3$ mm, and $\epsilon = 10$.

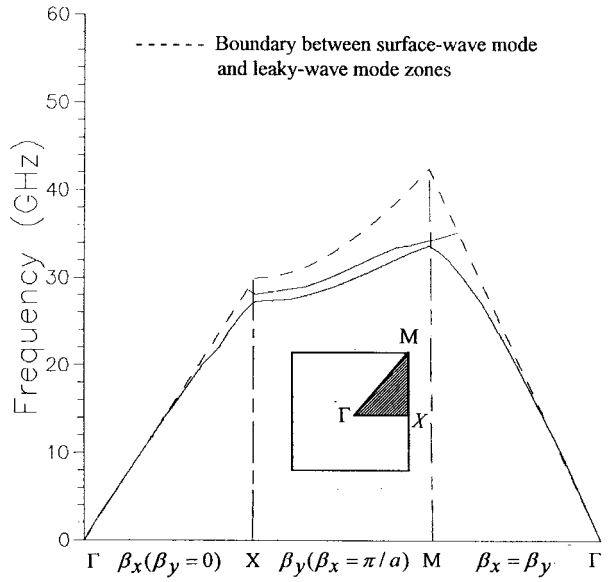

Fig. 11. Photonic band structures for the surface-wave modes of planar periodic dielectric blocks on a ground plane. All the parameters are the same as those in Fig. 9.

The photonic band structures for the bounded (slow-wave) modes of the structure in Fig. 10 is shown in Fig. 11. In the diagram, between Γ and X points, the modes are propagating in the $\hat{x}$ direction, while between M and Γ points, the modes are propagating in the $\hat{x}+\hat{y}$ direction. The shadow region in the inset of Fig. 11 is the irreducible Brillouin zone (reciprocal lattice). The dotted envelope in Fig. 11 corresponds to the plot for $\beta = k_0$, the boundary between guided (slow-wave) modes and leaky-wave (fast-wave) modes. In between X and M points, the bounded waves satisfy the Bragg condition in the $\hat{x}$ direction. At the M point, the guided waves satisfy the Bragg condition in the $\hat{x}+\hat{y}$ direction. From Fig. 11, one can see that there exists a photonic band-gap near the X point for guided wave in the $\hat{x}$ direction. Similar observation is also found in [2], [19] for the linear grating case. Photonic band-gaps are also found in other directions of propagation as shown in Fig. 11. Those band-gaps occur at different frequencies and there is no common frequency where all the band-gaps exist. This implies that complete surface-wave elimination is not possible in this example.

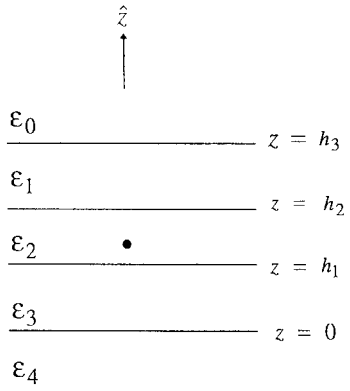

Fig. 12. A δ current source in a three-layer structure. The geometry is for Green's function derivation.

V. Conclusion

In this paper, through the use of a volume integral-equation analysis, guided-wave and leaky-wave characteristics of multilayer thin-film structures with planar material gratings were investigated. The results are validated by comparison with effective-medium approximation in low frequencies and in the limiting case against the linear grating cases. In this paper, it was found that there exists an angle range in the planar direction where guided waves (surface waves) are prohibited. The surface-wave forbidden zones shift with frequencies. For the open planar geometry, a complete photonic band-gap is not found. An angular-dependent photonic band-gap and band structures of planar grating structures are identified. The planar surface-wave patterns can be tailored by proper design of the planar gratings in a thin-film structure. This feature finds applications in high-directivity surface-wave antennas and space-frequency signal selectors. The leaky waves supported by the planar grating structures can be designed for high-gain integrated antennas [20]. The leak-wave beam angle as functions of frequency and grating parameters were investigated. The single-beam frequency band were also identified. It was found that there may also exist wave forbidden zones for leaky waves and the beam angle varies with the ϕ angle.

Appendix
Spectral Matrix Method for Green's Function in Layered Media

For the pertinent problem, the spectral Green's function is the spectral electric field due to a δ-current source embedded within the middle layer as shown in Fig. 12. We may define a

4×1 matrix $[\Psi(z)]$ for the spectral tangential fields as

$$[\Psi(z)] = \begin{bmatrix} k_x\tilde{H}_x + k_y\tilde{H}_y \\ k_y\tilde{H}_x - k_x\tilde{H}_y \\ k_x\tilde{E}_x + k_y\tilde{E}_y \\ k_y\tilde{E}_x - k_x\tilde{E}_y \end{bmatrix}. \tag{12}$$

Tangential fields in a homogeneous half-space can be derived as a linear combination of TE and TM waves that satisfy the Sommerfeld's radiation condition [13]. As a result, the tangential-field vector at the top and the bottom region in Fig. 12 can be found as

$$[\Psi(z)] = \begin{bmatrix} q_0\tilde{A} \\ -j\omega\varepsilon_0\tilde{B} \\ q_0\tilde{B} \\ j\omega\mu_0\tilde{A} \end{bmatrix} e^{-q_0(z-h_3)}, \quad z \geq h_3 \tag{13}$$

and

$$[\Psi(z)] = \begin{bmatrix} -q_4\tilde{C} \\ -j\omega\varepsilon_0\tilde{D} \\ -q_4\tilde{D} \\ j\omega\mu_0\tilde{C} \end{bmatrix} e^{q_4 z}, \quad z \leq 0 \tag{14}$$

if the structure is supported by a dielectric half-space, and

$$[\Psi(z=0)] = \begin{bmatrix} \tilde{C} \\ \tilde{D} \\ 0 \\ 0 \end{bmatrix} \tag{15}$$

if the structure is backed by a perfect conductor. $\tilde{A}$, $\tilde{B}$, $\tilde{C}$, and $\tilde{D}$ are unknowns to be determined, $q_0 = \sqrt{k_x^2 + k_y^2 - k_0^2}$ and $q_i = \sqrt{k_x^2 + k_y^2 - \varepsilon_i k_0^2}$, $i = 1, 2, 3$, or 4. If the tangential fields in the homogeneous-layered media are derived in terms of a linear combination of TE and TM waves, a transition matrix within each layer may be obtained as

$$[\Psi(z)] = [T_i(z - z_0)][\Psi(z_0)] \tag{16}$$

where

$$[T_i(z)] = \begin{bmatrix} \cosh q_i z & 0 & 0 & \tau_1 \sinh q_i z \\ 0 & \cosh q_i z & \tau_2 \sinh q_i z & 0 \\ 0 & \dfrac{1}{\tau_2}\sinh q_i z & \cosh q_i z & 0 \\ \dfrac{1}{\tau_1}\sinh q_i z & 0 & 0 & \cosh q_i z \end{bmatrix} \tag{17}$$

$\tau_1 = -(q_i/j\omega\mu_0)$, and $\tau_2 = j\omega\varepsilon_0\varepsilon_i/q_i$ with $i = 1$, 2, or 3. The unknowns $\tilde{A}$, $\tilde{B}$, $\tilde{C}$, and $\tilde{D}$ are found from the following matrix equations:

$$\begin{aligned}&[T_2(z' - h_2)][T_3(h_2 - h_3)][\Psi(h_3)] \\ &\quad - [T_2(z' - h_1)][T_1(h_1)][\Psi(0)] = [\tilde{J}].\end{aligned} \tag{18}$$

z' is the location of the δ source and $[\tilde{J}]$ is related to the source excitation

$$[\tilde{J}] = \begin{bmatrix} -k_y \\ k_x \\ 0 \\ 0 \end{bmatrix}, \quad \begin{bmatrix} k_x \\ k_y \\ 0 \\ 0 \end{bmatrix}, \quad \text{or} \quad \begin{bmatrix} 0 \\ 0 \\ k^2 \\ \hline \omega\varepsilon_0\varepsilon_2 \\ 0 \end{bmatrix} \tag{19}$$

for the δ source in the $\hat{x}$, $\hat{y}$, or $\hat{z}$ direction, respectively [21]. The solutions of (18) together with the transition matrix $[T_i(z)]$ allows one to determine the spectral fields at any location within the layered media. To ensure that (18) is invertable numerically for large m or n in practice, depending on the location of the field point, (18) is rearranged into two different forms. For $z' \geq z$ there is

$$\begin{aligned}&[T_3(h_2 - h_3)][\Psi(h_3)] - [T_2(h_2 - h_1)][T_1(h_1)][\Psi(0)] \\ &\quad = [T_2(h_2 - z')][\tilde{J}]\end{aligned} \tag{20}$$

and

$$[\Psi(z)] = [T_2(z - h_1)][T_1(h_1)][\Psi(0)]. \tag{21}$$

For $z \geq z'$ there is

$$\begin{aligned}&[T_2(h_1 - h_2)][T_3(h_2 - h_3)][\Psi(h_3)] - [T_1(h_1)][\Psi(0)] \\ &\quad = [T_2(h_1 - z')][\tilde{J}]\end{aligned} \tag{22}$$

and

$$[\Psi(z)] = [T_2(z - h_2)][T_3(h_2 - h_3)][\Psi(h_3)]. \tag{23}$$

The integration of the spectral Green's function over z and z' shown in (9) is a necessary procedure in the volume integral-equation analysis. This integration is directly related to the integration over (20) and (21), or (22) and (23), depending on locations of the source and field points. It is possible to perform the integration analytically. This detail is omitted here. Equation (17) can be normalized by dividing $\cosh q_i z$. The $\cosh$ terms, which grow exponentially, can be absorbed into unknowns $\tilde{A}$, $\tilde{B}$, $\tilde{C}$, and $\tilde{D}$. As a result, all the terms and matrix inversion are well behaved.

ACKNOWLEDGMENT

The author would like to thank Prof. D. R. Jackson at the University of Houston for helpful discussions on leaky waves.

REFERENCES

[1] E. Yablonovitch, "Photonic band-gap structures," *J. Opt. Soc. Amer. B, Opt. Phys.*, vol. 10, no. 2, pp. 283–294, Feb. 1993.

[2] S. T. Peng, T. Tamir, and H. Bertoni, "Theory of periodic dielectric waveguides," *IEEE Trans. Microwave Theory Tech.*, vol. MTT-23, pp. 123–133, Jan. 1975.

[3] T. Itoh and A. Hebert, "Simulation study of electronically scannable antennas and tunable filters integrated in a quasiplanar dielectric waveguide," *IEEE Trans. Microwave Theory Tech.*, vol. MTT-26, pp. 987–991, Dec. 1978.

[4] E. W. Lucas and T. P. Fontana, "A 3-D hybrid finite element/boundary element method for the unified radiation and scattering analysis of general infinite periodic arrays," *IEEE Trans. Antennas Propagat.*, vol. 43, pp. 145–153, Jan. 1995.

[5] H. Y. D. Yang, N. G. Alexopoulos, and R. Dias, "Reflection and transmission of waves from artificial-material layers made of periodic material blocks," in *IEEE Int. Symp. Antennas Progagat. Dig.*, Baltimore, MD, July 1996, pp. 1428–1431.

[6] C. F. Yang, W. D. Burnside, and R. C. Rudduck, "A double periodic moment method solution for the analysis and design of an absorber covered wall," *IEEE Trans. Antennas Progagat.*, vol. 41, pp. 600–601, May 1993.

[7] W. Sun, K. Liu, and C. A. Balanis, "Analysis of singly and doubly periodic absorbers by frequency-domain finite difference method," *IEEE Trans. Antennas Progagat.*, vol. 44, pp. 798–805, June 1996.

[8] W. Platte, "Spectral dependence of light-induced microwave reflection coefficient from optoelectronic waveguide gratings," *IEEE Trans. Microwave Theory Tech.*, vol. 43, pp. 106–111, Jan. 1995.

[9] S. D. Gedney, J. F. Lee, and R. Mittra, "A combined FEM/MoM approach to analyze the plane wave diffraction by arbitrary gratings," *IEEE Trans. Microwave Theory Tech.*, vol. 40, pp. 363–370, Feb. 1992.
[10] S. I. Pereverzev and P. Y. Ufimtsev, "Permittivity and permeability of a fiber grating," *Electromagnetics*, no. 14, pp. 137–151, 1994.
[11] W. P. Pinello, R. Lee, and A. C. Cangellaris, "Finite element modeling of electromagnetic wave interactions with periodic dielectric structures," *IEEE Trans. Microwave Theory Tech.*, vol. 42, pp. 2294–2301, Dec. 1994.
[12] D. M. Pozar and D. H. Schaubert, "Scan blindness in infinite arrays of printed dipoles," *IEEE Trans. Antennas Progagat.*, vol. AP-32, pp. 602–608, June 1984.
[13] J. L. Tsalamengas and N. K. Uzunoglu, "Radiation from a dipole in the proximity of a general anisotropic grounded layer," *IEEE Trans. Antennas Progagat.*, vol. AP-33, pp. 165–172, Feb. 1985.
[14] E. F. Kuester and C. L. Holloway, "Comparison of approximations for effective parameters of artificial dielectric," *IEEE Trans. Microwave Theory Tech.*, vol. 38, pp. 1752–1755, Nov. 1990.
[15] ———, "A low-frequency model for wedge or pyramid absorber arrays-I: Theory," *IEEE Trans. Electromag. Compat.*, vol. 36, pp. 300–306, Nov. 1994.
[16] H. Y. Yang and J. A. Castaneda, "Printed dipole characteristics in a two-layer geometry with uniaxial anisotropy," *Electromagnetics*, vol. 9, no. 4, pp. 439–450, 1989.
[17] N. W. Ashcroft and N. D. Mermin, *Solid State Physics.* New York: Saunders College Publishing, 1976.
[18] H. Y. D. Yang, "Finite difference method for 2-D photonic crystals," *IEEE Trans. Microwave Theory Tech.*, vol. 44, pp. 2688–2695, Dec. 1996.
[19] H. Stoll and A. Yariv, "Coupled-mode analysis of periodic dielectric waveguides," *Opt. Commun.*, vol. 8, no. 1, pp. 5–7, May 1973.
[20] H. Y. D. Yang, N. G. Alexopoulos, and E. Yablonovitch, "Photonic band-gap materials for high-gain printed circuit antennas," *IEEE Trans. Antennas Progagat.*, vol. 45, pp. 185–187, Jan. 1997.
[21] H.-Y. Yang, J. A. Castaneda, and N. G. Alexopoulos, "Surface wave modes of printed circuit on ferrite substrates," *IEEE Trans. Microwave Theory Tech.*, vol. 40, pp. 613–621, Apr. 1992.

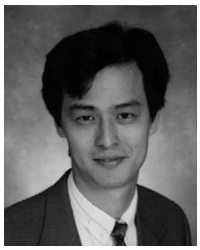

Hung Yu David Yang (S'87–M'88–SM'93) received the B.S. degree in electrical engineering from the National Taiwan University, Taipei, Taiwan, and the M.S. and Ph.D. degrees in electrical engineering from the University of California, Los Angeles (UCLA), in 1982, 1985, and 1988, respectively.

From 1988 to 1992, he was with Phraxos Research and Development, Inc. as a Research Engineer. There he was involved in the development of computer codes for frequency-selective surfaces, scattering-form antennas, design of microstrip antenna arrays, and antennas on nonreciprocal materials. Since August 1992, he has been an Assistant Professor in the Electrical Engineering and Computer Science Department, University of Illinois at Chicago. He serves as an Associate Editor of IEEE TRANSACTIONS ANTENNAS AND PROPAGATION since 1995, and a Technical Program Member of IEEE Microwave Symposium since 1994. He has published more than 60 journal and conference papers. His recent research interest has been on the development of computational methods for radiation and scattering from artificial periodic materials, vector integral-equation method and frequency-domain finite-difference method for photonic band-gap structures and advanced materials, wave interaction with bianisotropic media, and printed circuits and antennas on gyrotropic media.

Dr. Yang is a Member of URSIA Commission B and Sigma Xi.